European Cells and Materials Vol.58 2026 (pages 181–198) DOI: 10.22203/eCM.v058a13 ISSN 1473-2262

Original Article

Extracellular Matrix-Mimicking Dual-Network Hydrogel With Microenvironment Remodeling to Enhance Vascularized Skeletal Muscle Regeneration Following Volumetric Muscle Loss

Hanchen Liu[1,§], Jing Tao[2,§], Fengcheng Chu[1], Qiang Wang[2], Chen Wu[1], Kaichen Wan[1], Zhiwei Chai[2], Munan Guo[1], Hancheng Shi[1], Wei Yu[1], Xiao Lin[1], Fangsheng He[2], Huiling Liu[1,*] and Yixing Tian[1,2,*]

[1]Department of Orthopedics, The First Affiliated Hospital of Soochow University, Orthopedic Institute, Soochow University, 215006 Suzhou, Jiangsu, China

[2]Department of Orthopedic Center, Shihezi General Hospital of the Eighth Division, 832000 Shihezi, Xinjiang, China

[§]These authors contributed equally.

Abstract

Background: Volumetric muscle loss (VML) significantly impairs the inherent regenerative ability of skeletal muscle, causing dysfunction and scar tissue formation. Current treatments are limited to functional muscle transplantation, posing many complications and incomplete functional recovery. **Methods:** To simulate the extracellular matrix microenvironment and promote vascularized muscle regeneration, we developed a bioactive composite hydrogel with the angiogenic and myogenic effect of strontium ions (Sr^{2+}) and collagen type I (COL I), polyvinyl alcohol (PVA)/tannic acid (TA)/COL I/Sr^{2+} (PTCS). The physical properties of PTCS were characterized, including the mechanical properties, degradation, and release behavior. The *in vitro* influences of PTCS on C2C12 myoblasts and human umbilical vein endothelial cells (HUVECs) were evaluated via Cell Counting Kit-8, Live/Dead staining, wound healing, myotube differentiation, and Transwell assays. In addition, PTCS was implanted in the rat VML model and assessed for its effect on muscle regeneration *in vivo*. **Results:** The modulus of PTCS was similar to that of native rat muscle, and the degradation matched the muscle regeneration timeline. Controlled release of Sr^{2+} and COL I created a favorable microenvironment for vascular and muscular regeneration. PTCS facilitated the proliferation, migration, and differentiation of C2C12 myoblasts and enhanced the migration and invasion of HUVECs. Furthermore, the therapeutic effects of PTCS *in vivo* demonstrated a promoted vascular-specific marker CD31 expression, muscle fibers regeneration, and a decreased fibrosis area. **Conclusions:** These findings demonstrated that PTCS was a promising implantable biomimetic scaffold in skeletal muscle tissue engineering, and Sr^{2+} had a synergistic effect with COL I in muscle regeneration.

Keywords: Volumetric muscle loss, strontium, ionic hydrogel, angiogenesis, tissue engineering.

***Address for correspondence**: Yixing Tian, Department of Orthopedics, The First Affiliated Hospital of Soochow University, Orthopedic Institute, Soochow University, 215006 Suzhou, Jiangsu, China; Department of Orthopedic Center, Shihezi General Hospital of the Eighth Division, 832000 Shihezi, Xinjiang, China. E-mail: tianyixing@suda.edu.cn; Huiling Liu, Department of Orthopedics, The First Affiliated Hospital of Soochow University, Orthopedic Institute, Soochow University, 215006 Suzhou, Jiangsu, China. E-mail: liuhuilinghz@suda.edu.cn.

Introduction

Skeletal muscle tissue, the predominant tissue in the human body, plays a fundamental role in numerous physiological functions and movements [1]. Skeletal muscle possesses an inherent ability to regenerate in response to minor injuries. However, severe trauma and the associated surgical procedures often cause large-sized volumetric muscle loss (VML), characterized by damage exceeding 20 % of muscle volume. The innate capacity for regeneration is compromised permanently, leading to structural and functional impairment of patients and even heavy economic and social stress [2]. For example, 65 % of veterans with orthopedic trauma are estimated to be affected by large-sized VML, with associated disability costs exceeding 300,000 USD per person [3,4]. The prevailing clinical approach to managing VML is largely based on autologous tissue transplantation; however, postoperative complications such as infection, necrosis, and poor blood supply remain signifi-

cant challenges, and the limited availability of donor tissues constrains the restoration of skeletal muscle function [5]. Thus, developing an alternative treatment to re-establish the natural regeneration and restore function after VML injuries is clinically necessary.

Simulating the extracellular matrix (ECM) to construct a biomimetic scaffold with suitable mechanical behaviours and biocompatible microenvironment, thereby facilitating muscle regeneration, represents a promising approach for repairing large-volume muscle defects [6]. Hydrogels, which are three-dimensional networks of hydrophilic polymers, have garnered considerable attention for the regeneration and repair of various tissues, including skeletal muscles. Collagen type I (COL I) is a fundamental component of decellularized extracellular matrix (dECM) with favourable biocompatibility, rendering it an optimal raw material for hydrogel. What's more, COL I-based hydrogels have been widely recognized as an excellent biomaterial for vascularized tissue engineering [7]. Notably, COL I has been shown to play a critical role in enhancing the migration and myogenic differentiation of C2C12 myoblasts, highlighting its therapeutic potential in skeletal muscle regeneration [8]. Furthermore, Carleton *et al*. [9] demonstrated that COL I hydrogels could significantly promote muscle strength recovery and re-innervation in mice following severe skeletal muscle injury *in vivo*. However, the inherent mechanical weakness and high degradation of COL I-based hydrogel significantly restrict its potential applications in muscle tissue engineering. To further address these limitations, polyvinyl alcohol (PVA) was incorporated to form a double-network structure to enhance mechanical stability without compromising the biological activity of COL I because PVA is a synthetic polymer that could form a stable crosslinked-network through hydrogen bonding. In addition, tannic acid (TA), a natural polyphenol, was introduced as a crosslinker to the system. TA strengthens the network by hydrogen bonding and hydrophobic interactions, reducing the degradation rate of the collagen network [10,11]. This composite design aims to better mimic the native ECM microenvironment and provides both mechanical and biochemical cues conducive to skeletal muscle regeneration.

More importantly, skeletal muscle is a highly vascularized tissue, requiring a vascular network to provide sufficient oxygen and nutrients [12]. Angiogenesis has been demonstrated to precede myogenesis during skeletal muscle regeneration [13]. Therefore, developing a bioactive scaffold capable of rapidly vascularized regeneration at the injury site has been demonstrated as a promising approach to enhance skeletal muscle repair through the timely delivery of nutrients and oxygen to surrounding cells [14]. Currently, applying bio-functional ions in a scaffold to reconstruct blood vessels and thereby promote tissue repair is an effective strategy by modulating biological responses [15]. Among these, strontium ions (Sr^{2+}) have been used to enhance angiogenesis in a variety of tissues, including bone and skin, because it is known to possess angiogenic activity [16]. Yuan *et al*. [17] have demonstrated that Sr^{2+} can promote myofibroblast proliferation, suggesting sustained Sr^{2+} release from hydrogels may create a favourable microenvironment to stimulate myofiber formation. However, the therapeutic efficacy of Sr^{2+} in promoting the regeneration of vascularized skeletal muscle remains uncertain. Hence, Sr^{2+} was incorporated into the PVA/TA/COL I composite hydrogel, holding promise for enhancing skeletal muscle repair and vascularized regeneration via sustained releasing of COL I and Sr^{2+}.

At present, collagen hydrogels for VML repair rarely achieve both muscle-like mechanical properties and a degradation rate aligned with the muscle regeneration period [18]. In addition, the role of Sr^{2+} in muscle regeneration and its potential synergy with COL I have not been fully explored. Herein, a novel polyvinyl alcohol/tannic acid/COL I/Sr^{2+} (PTCS) scaffold was prepared, and we hypothesize that the hydrogel could simulate the mechanical environment of the ECM and mimic the physiological conditions of the ECM through the synergistic work of Sr^{2+} and COL I during the degradation process. The structure and the physical performance of the composite hydrogel were thoroughly evaluated firstly. Following this, the myogenesis-promoting function and angiogenesis-promoting capability of the PTCS were systematically evaluated *in vitro* and *in vivo* and compared with hydrogel scaffolds containing a single element to elucidate the synergistic effect of Sr^{2+} and COL I on skeletal muscle repair (Fig. 1).

Materials and Methods

Preparation and Characterization of the Hydrogels

Fabrication Procedure

COL I (S12007) was purchased from Yuanye Biotechnology Co., Ltd. (Shanghai, China). TA (T292288), PVA (P105126), and $SrCl_2 \cdot 6H_2O$ (S110516) were obtained from Aladdin Scientific Co., Ltd. (Shanghai, China). All chemicals were used without further purification. The deionized (DI) water was prepared in the laboratory. A composite hydrogel was prepared as follows: 4 wt% PVA and 1 wt% TA were dissolved in DI water at 95 °C for 3 hours. Subsequently, 1 wt% $SrCl_2 \cdot 6H_2O$ was added into the PVA/TA solution and stirred continuously for 30 min. After cooling, 8 wt% COL I was added and stirred until well blended. Finally, the mixed solution was frozen at –20 °C for 8 hours, and then thawed at room temperature for 2 hours. The freezing/thawing process was repeated three times to form the hydrogel (for short PTCS). Other composite hydrogels, including PVA (4 wt%), PVA/TA (PT, PVA 4 wt%, TA 1 wt%), PVA/TA/COL I (PTC, PVA 4 wt%, TA 1 wt%, COL I 8 wt%), and PVA/TA/$SrCl_2$ (PTS, PVA 4 wt%, TA 1 wt%, $SrCl_2 \cdot 6H_2O$ 1 wt%), were prepared according to the above method.

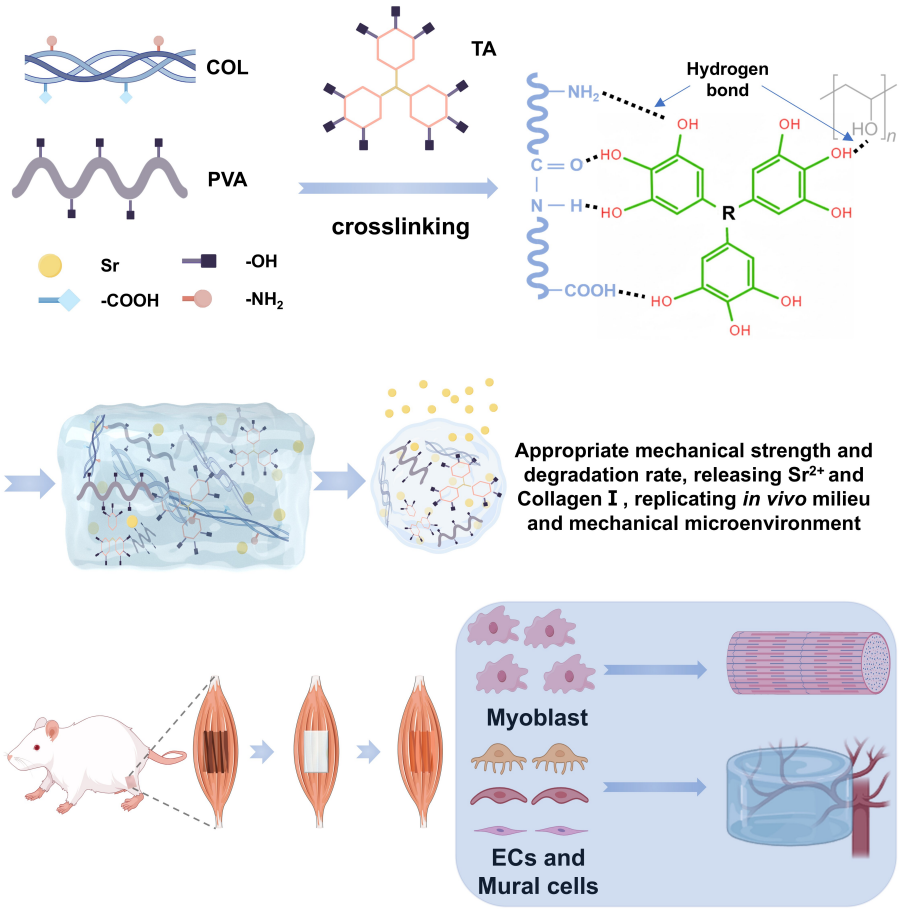

Fig. 1. Schematic illustration of fabricating COL I-based strontium ion-releasing hydrogels for the vascularized muscle regeneration. Fig. 1 is created in Figdraw (Figdraw company, China). COL I, collagen type I; PVA, polyvinyl alcohol; TA, tannic acid.

Microstructure

First, the hydrogel samples were freeze-dried thoroughly in a lyophilizer. Upon brittle fracturing, the internal structure was exposed and sputter-coated using an ion-sputter coating instrument (SC7620, Quorum, UK). Then the microstructure was observed at 5-15 kV through a scanning electron microscope (SEM, Axia Chemi, Thermo Fisher Scientific, USA). Porosity was calculated according to **Supplementary Equation 1**.

Phase Composition

To understand the major functional groups in hydrogels, the infrared spectra of the samples were acquired using Fourier transform infrared spectroscopy (FTIR, Nicolet, Thermo Fisher Scientific, USA). Completely lyophilized samples were ground into a fine powder and mixed with 99 wt% potassium bromide. The mixed powder was compacted to form a sample slice. The scanning range was set to 600–400 cm^{-1}, and the resolution was set at 0.25 cm^{-1}.

The Hydrogel powder was characterized by X-ray diffraction (XRD, Empyrean, PANalytica, Netherlands) with Ni-filtered Cu-Kα radiation (λ = 1.54 Å). XRD patterns were collected at the diffraction angle 2θ of 10°–50° with a step-scan mode of 2°·min^{-1}. The crystallinity of the hydrogels was calculated according to **Supplementary Equation 2**.

Rheological Tests

The rheological properties of all hydrogels were characterized using a rheometer (AR2000, TA Instruments, USA) with a parallel–plate configuration (a plate diameter of 20 mm and a gap between plates of 1 mm) at oscillating mode. The samples were manufactured into sizable discs to match the rheometer geometry. Frequency sweep tests were performed from 0.1 Hz to 50 Hz at 37 °C and 1 % strain.

Mechanical Tests

The mechanical characterization of hydrogels was measured on a universal testing machine (HY-1080, Hengyi Precision Instrument, China). Dumbbell-shaped samples (50 mm × 3 mm × 3 mm) were prepared for tensile (stretch-

ing speed of 10 mm·min^{-1} and gauge length of 30 mm) testing. Before testing, all samples were fully hydrated, and the measurements were performed immediately after removal from the hydration medium at room temperature. Each group included three independent samples (n = 3), and the data are expressed as mean ± standard deviation (SD). Statistical differences were analyzed by one-way analysis of variance (ANOVA) followed by Tukey's multiple comparisons test, with $p < 0.05$ considered statistically significant.

Degradation and Swelling Behavior *in vitro*

Completely dried hydrogels were weighed as w_0. A mass of 1 g of hydrogel was added to 10 mL of phosphate-buffered saline (PBS, P1020, Solarbio, China) at pH = 7.2~7.4 and incubated at 37 °C for 1, 3, 5, 7, 14, and 28 days. The incubation solution was refreshed every other day. After incubation, the remaining hydrogel was completely dried and reweighed (w_1). The degree of degradation (Δw) was determined based on the lost weight divided by the initial weight and calculated using Equation (1).

$$\Delta w\,(\%) = \frac{w_0 - w_1}{w_0} \times 100\% \qquad (1)$$

The swelling behavior of hydrogels was evaluated as described in **Supplementary Equation 3**.

Ion Release Measurements

To select a suitable Sr^{2+} release concentration, different $SrCl_2 \cdot 6H_2O$ contents (0.5 wt%, 1.0 wt%, and 1.5 wt%) were applied to prepare different PTCS. Then, 1 g of hydrogels was added to 10 mL of PBS and incubated at 37 °C for 1, 3, 5, and 7 days. The incubation solution was refreshed every other day. The Sr^{2+} concentrations were measured using an inductively coupled plasma-optical emission spectrometer (Thermo Fisher X Series 2, USA).

Biocompatibility of Composite Hydrogels

The hydrogel extracts were prepared according to the ISO 10993–5 standard. The hydrogels were immersed in a high-glucose Dulbecco's modified Eagle's medium (DMEM, C2701, Beyotime, China) with 10 % (v/v) fetal bovine serum (FBS, A5256701, Gibco, USA) and 1 % (v/v) penicillin–streptomycin solution (C0222, Beyotime, China) at a concentration of 0.1 g·mL^{-1} for 24 hours. Then, the extracts were filtered, and the filtrates were sterilized and used for cell culturing. Regular cell culture media (a high-glucose DMEM with the same substances) were used as the control group. C2C12 myoblasts and human umbilical vein endothelial cells (HUVECs) were purchased from the Stem Cell Bank of the Chinese Academy of Sciences and cultured in strict accordance with the provided instructions.

C2C12 myoblasts and HUVECs were seeded in 96-well plates at a density of 4×10^3 cells per well and cultured with regular culture media for 24 hours. Subsequently, the original media was substituted with the hydrogel extract, and regular media was added to the control group. After 1 and 3 days, the cell viability was assessed using the Cell Counting Kit-8 (CCK-8) assay (A311-01, Vazyme, China) by measuring the absorbance of all samples at 450 nm with a microplate reader (Elx808, BioTek Instruments, USA).

C2C12 myoblasts and HUVECs were seeded in 24-well plates at a density of 1×10^4 cells per well and cultured in regular cell culture media for 24 hours. Similar to the above protocol, the media was replaced, and the cells were cultured for 1 and 3 days. The cells were stained using a LIVE/DEAD viability kit (L3224, Thermo Fisher Scientific, USA) and imaged using a fluorescence microscope (Zeiss Axovert 200M, Carl Zeiss, Germany).

Effects of Hydrogels on the Migration and Differentiation of C2C12 Myoblasts

C2C12 myoblasts were seeded in 6-well plates at a density of 5×10^4 cells per well and cultured to approximately 100 % confluency. A wound was inflicted in the cell monolayer, and the media was substituted with the hydrogel extract containing 1 % FBS. Optical images were obtained at 0, 12, and 24 hours using an optical microscope (Carl Zeiss, Germany). The migration area was measured using ImageJ, and the migration rate was calculated as the ratio of the initial area to the final area.

C2C12 myoblasts were seeded in 24-well plates at a density of 5×10^4 cells per well and cultured to approximately 90 % confluency. Subsequently, the cells were cultured in differentiation media containing 2 % horse serum (S9050, Solarbio, China) for 6 days.

For staining, the cells were fixed with 4 % paraformaldehyde (BL539A, Biosharp, China) for 20 min and permeabilized using 0.1 % Triton-X100 (P0096, Beyotime, China). Then, the cells were stained with rhodamine–phalloidin (R415, Thermo Fisher Scientific, China) and 4′,6-diamidino-2-phenylindole (62248, Thermo Fisher Scientific, China). The cells were observed using a fluorescence microscope (EVOS, Advanced Microscopy Group, USA).

Effects of Hydrogels on the Migration and Invasion of HUVECs

HUVECs were seeded in 6-well plates at a density of 2×10^4 cells per well and cultured to approximately 100 % confluency. A wound was inflicted in the cell monolayer, and the media was substituted with the hydrogel extract containing 1 % FBS. Optical images were obtained at 0, 12, and 24 hours using an optical microscope (Zeiss Axovert 200M, Carl Zeiss, Germany). The migration area was measured using ImageJ, and the migration rate was calculated as the ratio of the initial area to the final area.

Transwell assays were performed in a 24-well tran-

swell chamber. HUVECs were seeded in the upper chamber at a density of 5×10^4 cells per chamber with serum-free DMEM. The hydrogel extract was added to the lower chamber. Then, the upper chamber was immersed in the media and incubated for 12 hours. The non-migrated HUVECs were removed using a cotton swab. The migrated HUVECs were fixed with 4 % paraformaldehyde, stained with 0.2 % crystal violet (C0121, Beyotime, China), and observed using an inverted microscope. ImageJ was used to count the number of cells.

In vivo Implantation of Hydrogels Into the Rat Tibialis Anterior (RTA) Muscle Defect Model

Operation Procedure

The animal experiments were approved by the ethics committee of our University (SUDA20241014A01) according to the Planning Research and Experimental Procedures on Animals (PREPARE) and reported following the Animal Research: Reporting of In Vivo Experiments (ARRIVE) guidelines. Forty adult male Sprague-Dawley rats (8 weeks old, 280–300 g, Experimental Animal Centre of Soochow University) were randomly divided into five groups (n = 8 per group): (1) Untreated, (2) PT, (3) PTS, (4) PTC, and (5) PTCS. First, the rats were anesthetized using a 1 % pentobarbital sodium intraperitoneal injection (40 mg·kg^{-1}) at least 15 minutes before surgery. The animal model was produced by resecting the RTA muscle [19]. Before surgery, the hydrogels were prepared in a designed mold with the same dimension to ensure matching defects. First, an incision parallel to the tibia was made, and the fascia was bluntly dissected to expose the RTA muscle. Then, a piece of muscle (10 mm × 7 mm × 3 mm) was removed from the middle third of the muscle. After hemostasis, the hydrogels were implanted, and the fascia and skin were sutured. For the untreated group, no treatment was performed except suturing. After surgery, meloxicam (2 mg kg·d^{-1}) was administered subcutaneously for 3 days. The animals were sacrificed 28 days and 56 days post-operation by euthanasia, with n = 4 per group at each time point. Blinding was not feasible for the participants and care providers due to the nature of the interventions. However, the outcome assessors and data analysts were blinded to the group assignments.

Muscle Morphology and Weight

The RTA muscle was completely dissected bilaterally from rats, and the contralateral side served as the control. Morphological images were acquired using a camera. The TA muscle regeneration efficiency (w_m) was determined based on the injured RTA muscle weight (w_i) divided by the contralateral RTA muscle weight (w_c) and calculated using Equation (2).

$$w_m\,(\%) = \frac{w_i}{w_c} \times 100\% \qquad (2)$$

Histological Analysis

After being fixed in 10 % neutral formalin (R22054, YuanYe, China), the muscle specimens were dehydrated. Then, the specimens were embedded in paraffin blocks and sectioned at a thickness of 6 μm using a microtome, and the sections were subjected to hematoxylin and eosin (H&E) staining and Masson's trichrome (MT) staining. For immunohistochemical analysis, the sections were dewaxed, and the antigen was retrieved with citrate buffer. Subsequently, the samples were treated with 0.1 % Triton X-100 and 2 % bovine serum albumin (B14, Thermo Fisher Scientific, USA). Then, the sections were incubated overnight at 4 °C with the primary antibody CD31 (1:50, ab28364, Abcam, UK). Afterward, the tissue sections were incubated with biotin-conjugated secondary antibodies and avidin-biotin enzyme reagents for 30 min. Color development was achieved by using chromogen 3,3′-diaminobenzidine tetrahydrochloride (34002, Thermo Fisher Scientific, USA) and hematoxylin. Images were acquired using a Zeiss Axiocam microscope and analyzed using ImageJ software. Collagen fiber deposition was assessed in Masson staining by calculating the ratio of the blue-stained collagen area to the total tissue area. For CD31 staining, vascularization was quantified by measuring the CD31-positive area (μm^2 per field). All histological samples were assessed by two independent blinded outcome assessors. When the assessors differed in grading, this was discussed until consensus on the grade was reached.

Statistical Analysis

Data were statistically analyzed using GraphPad Prism (GraphPad software, USA, Version 10.1.2) and Origin Pro (OriginLab, USA, 10.3.0.180). A t-test was used to compare the two groups of samples. For multiple comparisons, one-way or two-way ANOVA with Tukey's post hoc test was employed. A value of $p < 0.05$ was considered statistically significant.

Results

Microstructure of Hydrogels

The SEM photographs clearly demonstrated the internal structure of the hydrogels. All hydrogels showed a typical sponge-like porous structure. The microstructure of PVA was a homogeneous network, and PTCS basically maintained its original characteristics (Fig. 2**A**). Quantitative SEM image analysis further supported these observations (**Supplementary Table 1** and **Supplementary Fig. 1**). The average pore size of PTCS was higher than that of PVA (PVA: 14.87 μm, PTCS: 50.35 μm), while the porosity reached 77.68 % for PTCS. PTCS displayed a broader, right-skewed distribution with 31.73 % of pores in the 50-100 μm range. Importantly, pore structure is closely related to the hydrogel's degradation and release behavior. PTCS with large pores and high porosity can allow fast water pen-

etration, facilitate erosion, accelerating mass loss [20]. The pore architecture also provided a structural basis for the burst release of Sr^{2+} at Day 1 [21].

The beneficial properties may be attributable to the hydrogen bonding interactions and crystalline regions in the hydrogels. TA provided the phenolic hydroxyl group to form hydrogen bonds with the hydroxyl group of PVA and the amide group of COL I [22]. Freeze-thaw cycling can cause phase separation and crystallization of PVA to produce microcrystalline junctions [23]. In PT formation, more hydrogen bonds supported larger ice domains, causing a larger pore size. Sr^{2+} or COL I can increase nucleation sites and restrict ice crystal growth, leading to small pores [24,25]. In PTCS, the Sr^{2+} decreased the entanglements of collagen to increase crystal formation [26]. The sponge-like microstructure can facilitate the transportation of nutrients and wastes when implanted *in vivo* [27].

Mechanical Properties of Hydrogels

The optimal stiffness of a hydrogel should match the requirements for myoblast attachment, proliferation, and differentiation. The rheological properties of the hydrogels are shown in Fig. 2**B**. The rheological properties of PT, PTC, PTS and PTCS were similar to those of PVA and all exhibited solid elastic gel properties, revealing a negligible impact on the modulus of Sr^{2+} and COL I. Notably, the storage modulus of PTCS was similar to the optimal modulus required to facilitate the maturation and alignment of muscle progenitor cells *in vitro* [28].

The mechanical properties of a hydrogel are an important parameter for implant materials. Fig. 2**C** and Table 1 display the main mechanical parameters of the hydrogels. The tensile strength of the pure PVA hydrogel was 61.07 ± 15.52 kPa, while introducing TA increased the tensile strength to 113.72 ± 4.59 kPa. Additionally, introducing TA enhanced the tensile modulus (PVA: 13.54 ± 2.46 kPa, PT: 20.04 ± 2.51 kPa) (Fig. 2**F**). The incorporation of COL I led to an improvement in the tensile modulus (PT: 20.04 ± 2.51 kPa, PTC: 28.30 ± 2.9 kPa), tensile strength (PT: 113.72 ± 4.59 kPa, PTC: 190.47 ± 9.55 kPa), and elongation at break (PT: 171.01 ± 14.44 %, PTC: 240.45 ± 21.83 %) (Fig. 2**F**, 2**G**, 2**H**). The addition of Sr^{2+} did not make any significant difference between PTS and PT, because low Sr^{2+} content cannot provide enough metal-phenolic junctions, and Sr^{2+} formed weak and unstable coordination crosslinks with TA [29]. The late addition of Sr^{2+} may also be a contributing factor. PTCS showed superior tensile properties, with a higher tensile strength (240.97 ± 25.91 kPa) and elongation at break (284.02 ± 9.99 %). The elastic modulus of native rat skeletal muscle ranges from 20 to 24.7 kPa [30,31]. Notably, all of our hydrogels were within this window, mimicking the mechanical microenvironment of skeletal muscle. Moreover, the elastic modulus of PTCS was 23.62 ± 0.58 kPa, approaching the stiffness of 21 kPa that optimally increased the proliferation of muscle satellite cells and mediated the maintenance and regeneration of muscle tissue [32].

XRD of Hydrogels

As shown in Fig. 2**D**, the XRD indicated that all hydrogels exhibited distinctive diffraction peaks within the 2θ range of 19°–21°, aligning with the (101) plane surface of PVA. The crystallinity of the hydrogels with added Sr^{2+} was reduced (PT: 58.90 %, PTS: 46.86 %, PTC: 44.36 %, PTCS: 40.55 %), because divalent ions such as Sr^{2+} and Ca^{2+} can disrupt the hydrogen bonds between PVA chains, and increase the amorphous fraction of the polymer, inhibiting the growth of PVA nanocrystals (**Supplementary Table 2**) [33,34]. The characteristic diffraction peaks of $SrCl_2 \cdot 6H_2O$ were not observed in the hydrogel samples, indicating that the $SrCl_2 \cdot 6H_2O$ recrystallization process was inhibited by the interactions of PVA and COL I during the lyophilization process.

FTIR of Hydrogels

Here, a COL I-Sr^{2+} dual-network composite hydrogel was prepared by incorporating $SrCl_2$ into a COL I/PVA/TA hydrogel matrix. This hydrogel was formed via strong hydrogen bonding between TA and PVA, as well as the crosslinking among the COL I chains without chemical crosslinking. The PVA/TA/COL I hydrogel was used as the ion carrier, and $SrCl_2$ was the source of Sr^{2+}.

The changes in chemical bonds were qualitatively evaluated using FTIR, as shown in Fig. 2**E**. The absorption peak of the O-H group exhibited a shift from 3372 cm^{-1} to 3366 cm^{-1}, indicative of robust hydrogen bond formation between PVA and TA. The amide I (1669–1638 cm^{-1}) and II (1550 cm^{-1}) bands in COL I are sensitive to the triple helix structure of COL I; thus, a notable shift in the position of these bands indicates a change in the molecular conformation of COL I. The amide I band shifted to a wavelength of 1650 cm^{-1}, while the position of the amide II band was not shifted. This suggests that the triple helix structure of COL I remains intact after cross-linking. New absorption peaks were observed at 1445 cm^{-1} and 1246 cm^{-1} and were attributed to the absorption peaks of C=C and C–O in TA, respectively. The FTIR analysis demonstrated that ingredients did not participate in any significant chemical cross-linking or reaction with each other. Instead, the gel was formed by physical cross-linking, including hydrogen bonding.

Ion Release Kinetics of Hydrogels

The regeneration effect of these hydrogels, when implanted *in vivo*, relied on the release of the Sr^{2+}. As shown in Fig. 2**I**, all hydrogels exhibited the capacity for sustained Sr^{2+} release. At the early stage, the released Sr^{2+} concentration increased with the amount of $SrCl_2 \cdot 6H_2O$ added to the hydrogel. For example, on the first day, the hydrogel group with 0.5 % $SrCl_2 \cdot 6H_2O$ (hereafter referred to as the

Table 1. The mechanical properties of all hydrogels.

Hydrogel	Tensile Modulus (kPa)	Tensile Strength (kPa)	Elongation at Break (%)
PVA	13.54 ± 2.46	61.07 ± 15.52	165.04 ± 15.80
PT	20.04 ± 2.51	113.72 ± 4.59	171.01 ± 14.44
PTC	28.30 ± 2.90	190.47 ± 9.55	240.45 ± 21.83
PTS	20.89 ± 1.32	109.83 ± 21.10	166.83 ± 8.25
PTCS	23.62 ± 0.58	240.97 ± 25.91	284.02 ± 9.99

PVA, polyvinyl alcohol; PT, PVA/TA; PTC, PVA/TA/COL I; PTS, PVA/TA/$SrCl_2$; PTCS, polyvinyl alcohol/tannic acid/COL I/Sr^{2+}.

0.5 % Sr group) released 6.49 ± 1.37 $\mu g \cdot mL^{-1}$. The 1 % Sr^{2+} group released 11.57 ± 0.62 $\mu g \cdot mL^{-1}$, and the 1.5 % Sr^{2+} group released 15.19 ± 0.67 $\mu g \cdot mL^{-1}$. The amount of Sr^{2+} in all groups decreased over time. On Day 7, all hydrogels released a similar quantity of Sr^{2+} at a concentration of approximately 3 $\mu g \cdot mL^{-1}$. These results indicate a time-dependent Sr^{2+} release behavior in the hydrogels.

Degradation and Swelling Behavior of Hydrogels in vitro

The degradation of the hydrogels was tested *in vitro* for up to 28 days to predict the tendency of hydrogels to degrade *in vivo* and match the rates of degradation and regeneration. The mass loss ratios of hydrogels at different time points are shown in Fig. 2**J**. The results indicated that all hydrogels were biodegradable. In PBS, the degradation of PVA is mainly attributed to erosion and disruption of the hydrogen bond instead of polymer chain scission. In the degradation process, water penetrated the network, disrupted the crosslink points and disentangled PVA chains, which dissolved into the medium [35]. The degradation rates of the PTC and PTCS groups exceed 80 % within 4 weeks, similar to the normal duration required for physiologic muscle healing. The COL I containing hydrogels degraded faster than the PT and the PTS group because part of COL I was physically entrapped in the network and could leach out during incubation, increasing the mass loss [36]. In addition, COL I competes with PVA for hydrogen bonding with TA, weakening the PVA network and accelerating erosion [37]. Meanwhile, this may reflect that the hydrogel with Sr^{2+} did not form new covalent crosslinks, consistent with the FTIR and XRD results. Notably, hydrogels containing COL I, such as PTC and PTCS, showed accelerated degradation rates, corroborating the expeditious degradation characteristics of COL I-based hydrogels documented in previous studies. The swelling results showed that after 24 hours, there is no significant difference between PT, PTS, and PTC (PT: 130 ± 0.7 %, PTC: 126.2 ± 4.4 %, PTS: 132.7 ± 6.27 %). PTCS has a swelling rate of 141.9 ± 2.76 %, which is higher than PT and PTC (**Supplementary Fig. 2**). Degradation of PTCS is higher than that of PTC, which is consistent with the degradation results. A higher swelling rate generally indicates an easier hydration, facilitating fractions leaching and structure erosion, which contributes to mass loss [38]. The rapid hydration and swelling caused a maximum Sr^{2+} release at the beginning, and then the network approached equilibrium hydration, exhibiting a subsequent reduction in release.

PTCS Promoted the Proliferation, Migration, and Myogenic Differentiation of C2C12 Myoblasts

C2C12 myoblasts were derived from mouse satellite cells and have been utilized extensively for assessing myogenic potential *in vitro* [39]. Accordingly, the biological effects of hydrogels were investigated on the proliferation, migration, and myogenic differentiation of C2C12 myoblasts. The findings demonstrated that all hydrogels exhibited favorable biocompatibility. The live/dead staining assays indicated a greater density of viable C2C12 myoblasts in the PTCS group than in the control group. PT, PTC, and PTS showed no significant difference (Fig. 3**A**). As shown in Fig. 3**D**, the optical density (OD) value of the PTCS group was elevated markedly compared with the control group at both Day 1 and Day 3, indicating that PTCS facilitated the proliferation of C2C12 myoblasts. The OD values of other groups did not differ significantly from the control group, indicating that PT, PTS, and PTC did not significantly affect the proliferation.

Furthermore, the effect of the hydrogels on the migration of C2C12 myoblasts was verified using the wound healing assay, which quantitatively measured the cell migration ability at 12 hours and 24 hours (Fig. 3**B**). At 12 hours, the cells did not migrate significantly into the scratched area except for the PTCS group. The quantitative analysis demonstrated that the migration rate in the PTCS group was 50 %, markedly higher than that in other groups. Notably, the cells maintained the same migration rate trend over a 24-hour period. In the PTCS group, the cells covered the scratched area, and the migration rate was approximately 75 %, however, the PTC group showed slightly accelerated C2C12 myoblast migration compared with the PT and control groups at 12 hours (Fig. 3**E**). These results indicated that the PTCS extract could significantly enhance the migration of C2C12 myoblasts.

For an in-depth study, the effects of hydrogel extracts on the myogenic differentiation of C2C12 myoblasts were evaluated. After 6 days, all groups exhibited obvious myotube formation (Fig. 3**C**). The quantitative analysis indicated that the widths of the myotubes in the PTC and PTCS

groups were higher than those in the control, PT, and PTS groups; however, no significant differences were observed between the control group and the PT and PTS groups (Fig. 3**F**).

PTCS Promoted the Migration and Invasion of HUVECs

HUVECs exhibit high proliferative capacity and form capillaries, rendering them a commonly utilized model for studying angiogenesis, a crucial process for vascularized muscle regeneration. The CCK-8 and live/dead staining assays demonstrated that the viability of HUVECs was comparable between the PTCS and control groups (Fig. 4**A**, 4**D**). The wound healing assay demonstrated that all hydrogels facilitated cell migration compared with the PT and control groups. Moreover, the stimulatory impact of PTCS was notably enhanced compared with that of PTC, indicating a potential synergistic effect of Sr^{2+} on cell migration (Fig. 4**B**, 4**E**). Furthermore, the Transwell assays exhibited that the invasion ability of HUVECs was increased significantly in the PTS and PTCS groups compared with those in other groups, indicating that the enhancement ability may be due to Sr^{2+} in the extract (Fig. 4**C**, 4**F**).

PTCS Improved Vascularized Muscle Regeneration in vivo

The RTA muscle defect model was selected to evaluate the ability of PTCS to promote vascularized skeletal muscle regeneration after VML *in vivo*. Considering the influence of COL I and Sr^{2+}, PT, PTC, PTS, and PTCS were screened for the capacity to induce muscle regeneration. At the same time, no treatment group was used as the control group.

After 28 days, all implanted hydrogels were completely degraded within 4 weeks, consistent with the normal duration required for physiological muscle healing [40]. Gross morphological observation at both 28 and 56 days revealed no obvious residual hydrogel, marked edema, or signs of infection, suggesting satisfactory *in vivo* tolerance of the hydrogels. The volume of the affected RTA muscle in the untreated and PT groups was significantly smaller than that of healthy RTA muscle, with the surface showing significant depressions and scar tissue. In the PTCS group, the affected RTA muscle was similar in volume to the healthy side, with more neoplastic tissue at the defect site and fuller muscle morphology. In contrast, the muscle showed limited regeneration in the PTC and PTS groups (Fig. 5**A**). After 56 days, the affected muscle in the PTCS group was similar to the healthy muscle. Statistical analysis revealed no significant difference in body weight between the groups of rats at either 4 or 8 weeks (Fig. 5**B**). The weight of RTA muscle in the PTCS group was similar to that of the contralateral muscle and increased significantly compared with the untreated and PT groups after 28 days and 56 days, indicating that PTCS was efficient in enhancing the regeneration of muscle morphology and weight (Fig. 5**C**).

Subsequently, H&E staining, MT staining, and immunohistochemical CD31 staining were conducted to assess myogenesis, fibrosis levels, and angiogenesis comprehensively. As shown in Fig. 5**D**, the H&E staining assay demonstrated that only a few centrally nucleated myofibers and excessive fibroblasts were observed in the untreated and PT groups, indicating the loss of regenerative ability. New myofibers with a central nucleus were identified at the implanted sites in the PTC, PTS, and PTCS groups, and the myofibers in the PTCS group exhibited greater thickness and regularity of shape compared with those in the PTC and PTS groups. The quantitative analysis demonstrated that the muscle in the PTCS group had the largest number of centrally nucleated myofibers. After 56 days, centrally nucleated myofibers were fewer than after 28 days, suggesting that the muscle fibers were maturing (Fig. 5**E**, 5**F**).

MT staining showed that after 28 days, blue collagen fibers were observed in all groups. The control and PT groups exhibited substantial fibrotic and adipose tissue deposition in the damaged areas. Additionally, intense collagen staining was identified in the defect sites of the PTC and PTS groups. In contrast, the deposition of collagen fiber in the PTCS group was diminished significantly. After 56 days, collagen fibers became more readily observable in the control and PT groups, indicating scar formation. In contrast, fewer collagen fibers were observed in the PTS, PTC, and PTCS groups (Fig. 6**A**). The quantitative analysis showed that the area of collagen fibers in the PTS, PTC, and PTCS groups was significantly lower than that in other groups (Fig. 6**B**, 6**C**).

CD31 staining indicated that the number of blood vessels at the injury site was minimal in both the control and PT groups, with the majority concentrated at the interface between scar tissue and muscle fibers (Fig. 6**D**). In comparison to the control group, the PTC group demonstrated a notable increase in vascular density. Meanwhile, the muscle defects in the PTS and PTCS groups, which contained Sr^{2+}, showed an elevated vascular density, accompanied by a fully developed vascular network. After 56 days, the lumen diameter was increased, with a marked increase in vascular infiltration, consistent with H&E staining. In addition, the quantitative analysis based on the CD31-positive area showed that the PTS, PTC, and PTCS groups had larger vascularization areas than the control and PT groups. Moreover, the vascularization area was significantly greater at 8 weeks than at 4 weeks. In contrast, the regions within the control and PT groups exhibited comparable levels at both time points (Fig. 6**E**, 6**F**).

Discussion

Tissue engineering is a promising approach for vascularized muscle regeneration because of its tailored mechanical properties and biofunctionalized structure. A variety of tissue engineering approaches have been developed for VML, with a significant improvement of muscle regen-

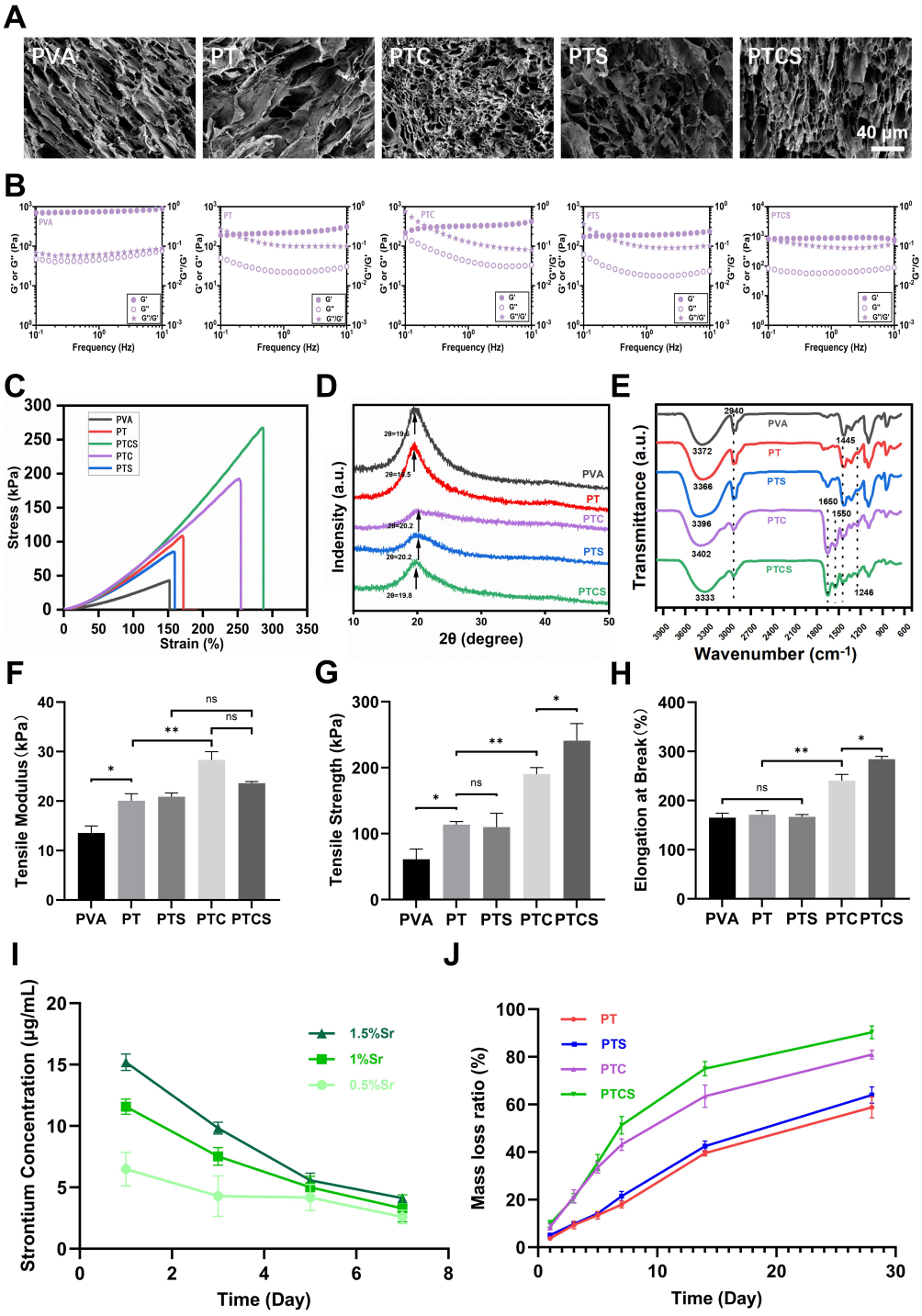

Fig. 2. Characterization of hydrogels. (**A**) Microstructure of hydrogels. Scale bars = 40 μm. (**B**) Dependence of G′, G″ and the G″/G′ ratio (loss factor) of hydrogels on the oscillation frequency. (**C**) Stress-strain curve of hydrogels. (**D**) XRD spectra of hydrogels. (**E**) FTIR spectra of hydrogels. (**F**) Tensile modulus of hydrogels. (**G**) Tensile strength of hydrogels. (**H**) Elongation at break of hydrogels. (**I**) Sr^{2+} concentrations in the immersion solution containing various Sr^{2+}-containing hydrogels for different periods. (**J**) Variation in the mass loss ratio of hydrogels with time when soaked in PBS for 28 days. All data are expressed as mean ± SD (n = 3). The exact *p* value in the above multiple comparisons was calculated with one-way ANOVA Tukey's multiple comparisons test. ns: no significant difference, *$p < 0.05$, **$p < 0.01$. PVA, polyvinyl alcohol; PT, PVA/TA; PTC, PVA/TA/COL I; PTS, PVA/TA/$SrCl_2$; PTCS, polyvinyl alcohol/tannic acid/COL I/Sr^{2+}; FTIR, Fourier transform infrared spectroscopy; XRD, X-ray diffraction; SD, standard deviation.

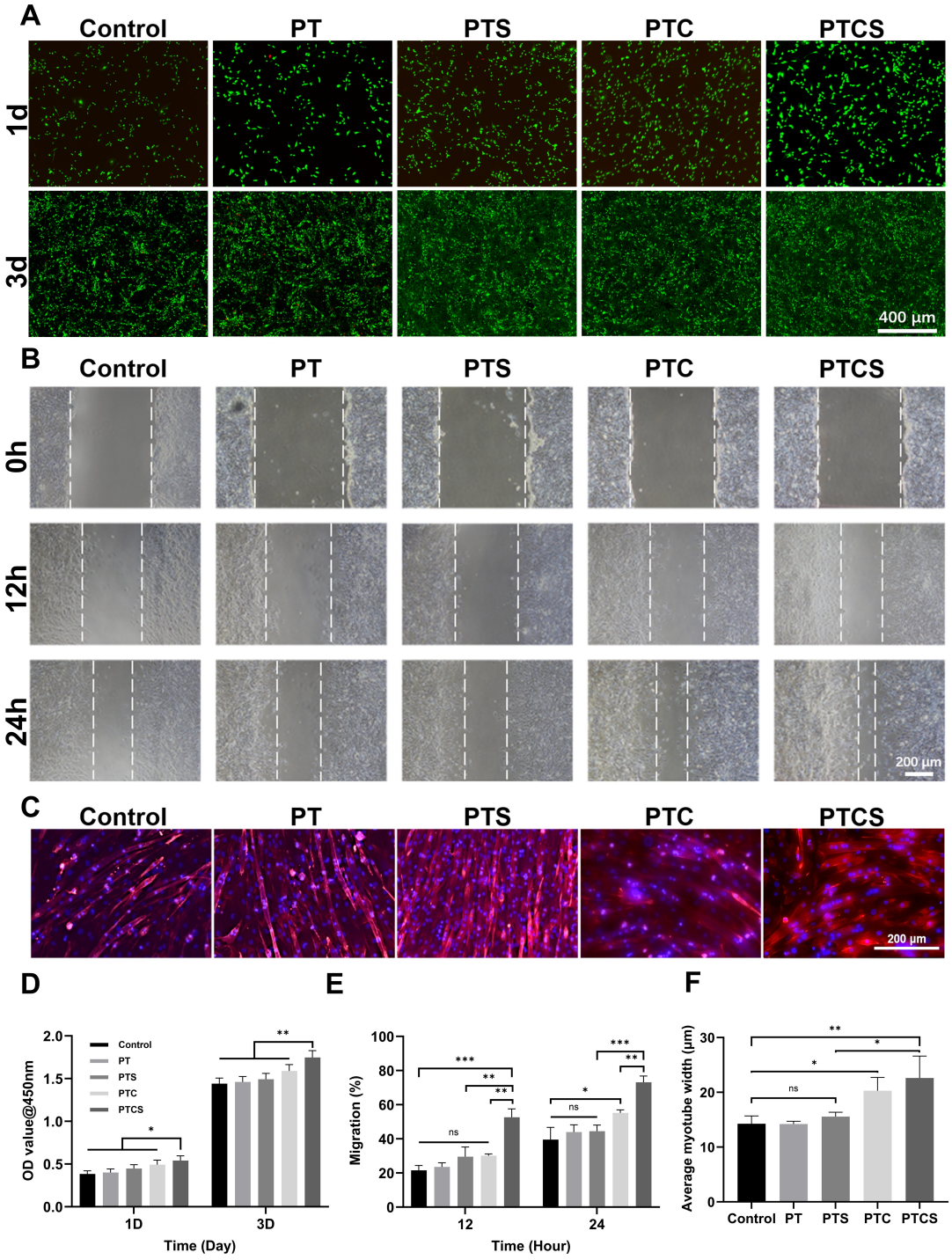

Fig. 3. PTCS promotes the proliferation, migration, and myogenic differentiation of C2C12 myoblasts. (**A**) Fluorescence micrographs of live/dead stained C2C12 myoblasts after culturing for 1 day and 3 days. Scale bars = 400 μm. (**B**) Representative micrographs of C2C12 myoblast migration when cultured for 0, 12, and 24 hours. Scale bars = 200 μm. (**C**) Actin filament staining (Phalloidin: red, DAPI: blue) of myotubes Scale bars = 200 μm. (**D**) OD values (450 nm) of the CCK-8 assay on C2C12 myoblasts cultured for 1 day and 3 days. (**E**) Quantification of the migration rate of different groups in the wound healing assay. (**F**) Quantification of the average myotube width of different groups. All data are expressed as mean ± SD (n = 3). The exact *p* value in the above multiple comparisons was calculated with one-way ANOVA Tukey's multiple comparisons test. ns: no significant difference, *$p < 0.05$, **$p < 0.01$, ***$p < 0.001$. PT, PVA/TA; PTC, PVA/TA/COL I; PTS, PVA/TA/$SrCl_2$; PTCS, polyvinyl alcohol/tannic acid/COL I/Sr^{2+}; OD, optical density; SD, standard deviation.

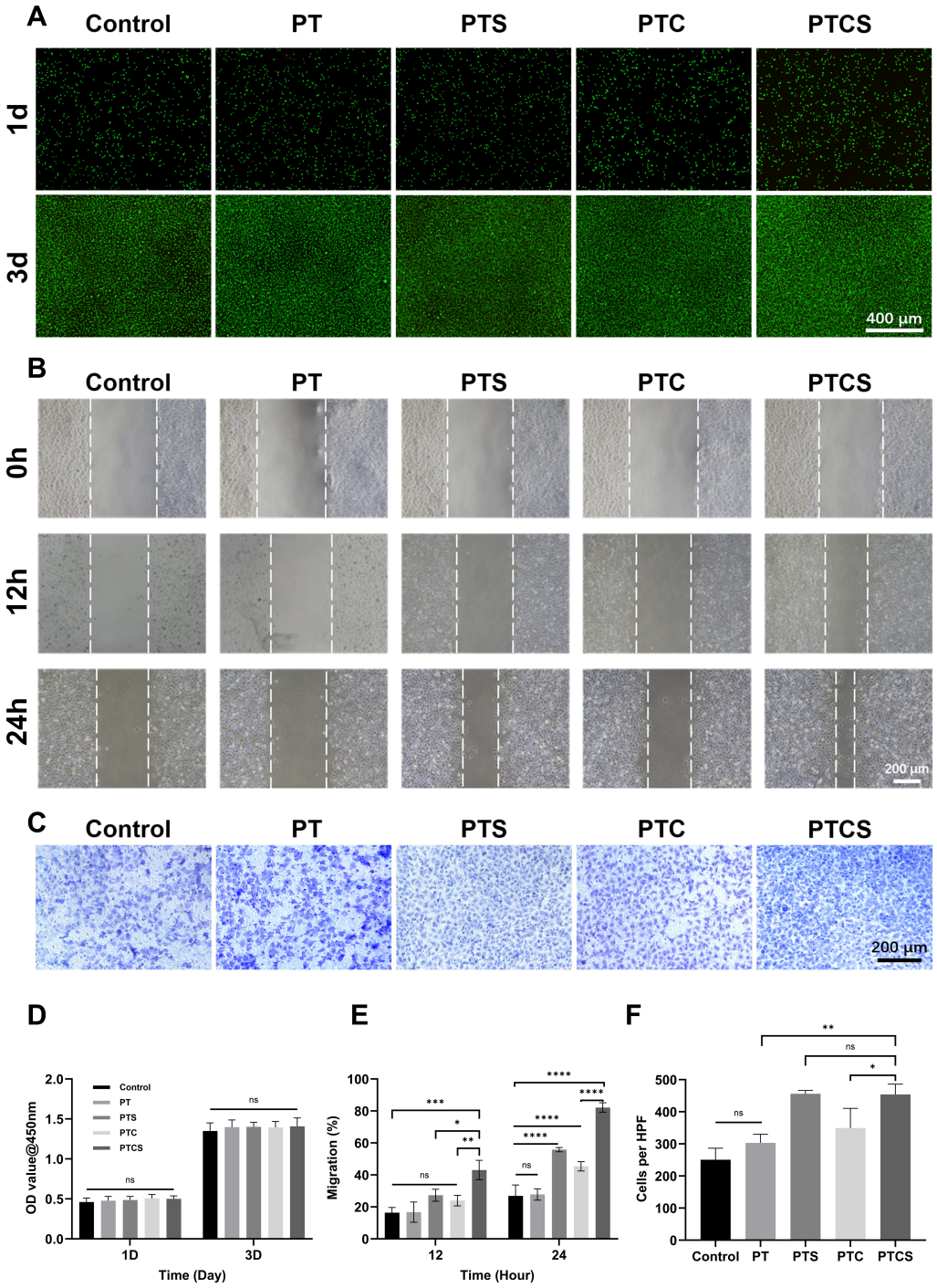

Fig. 4. PTCS promotes the migration and invasion of HUVECs. (**A**) Fluorescence micrographs of live/dead stained HUVECs. Scale bars = 400 μm. (**B**) Representative micrographs of HUVECs migration. Scale bars = 200 μm. (**C**) Transwell images of HUVECs that migrated to the lower chamber. Scale bars = 200 μm. (**D**) OD values (450 nm) of the CCK-8 assay on HUVECs cultured for 1 and 3 days. (**E**) Quantification of the migration rate of different groups in the wound healing assay. (**F**) The number of migrated HUVECs per high-power field was calculated by ImageJ in the Transwell assay. All data are expressed as mean ± SD (n = 3). The exact *p* value in the above multiple comparisons was calculated with one-way ANOVA Tukey's multiple comparisons test. ns: no significant difference, $*p < 0.05$, $**p < 0.01$, $***p < 0.001$, $****p < 0.0001$. PT, PVA/TA; PTC, PVA/TA/COL I; PTS, PVA/TA/$SrCl_2$; PTCS, polyvinyl alcohol/tannic acid/COL I/Sr^{2+}; OD, optical density; HUVECs, human umbilical vein endothelial cells; CCK-8, Cell Counting Kit-8; SD, standard deviation.

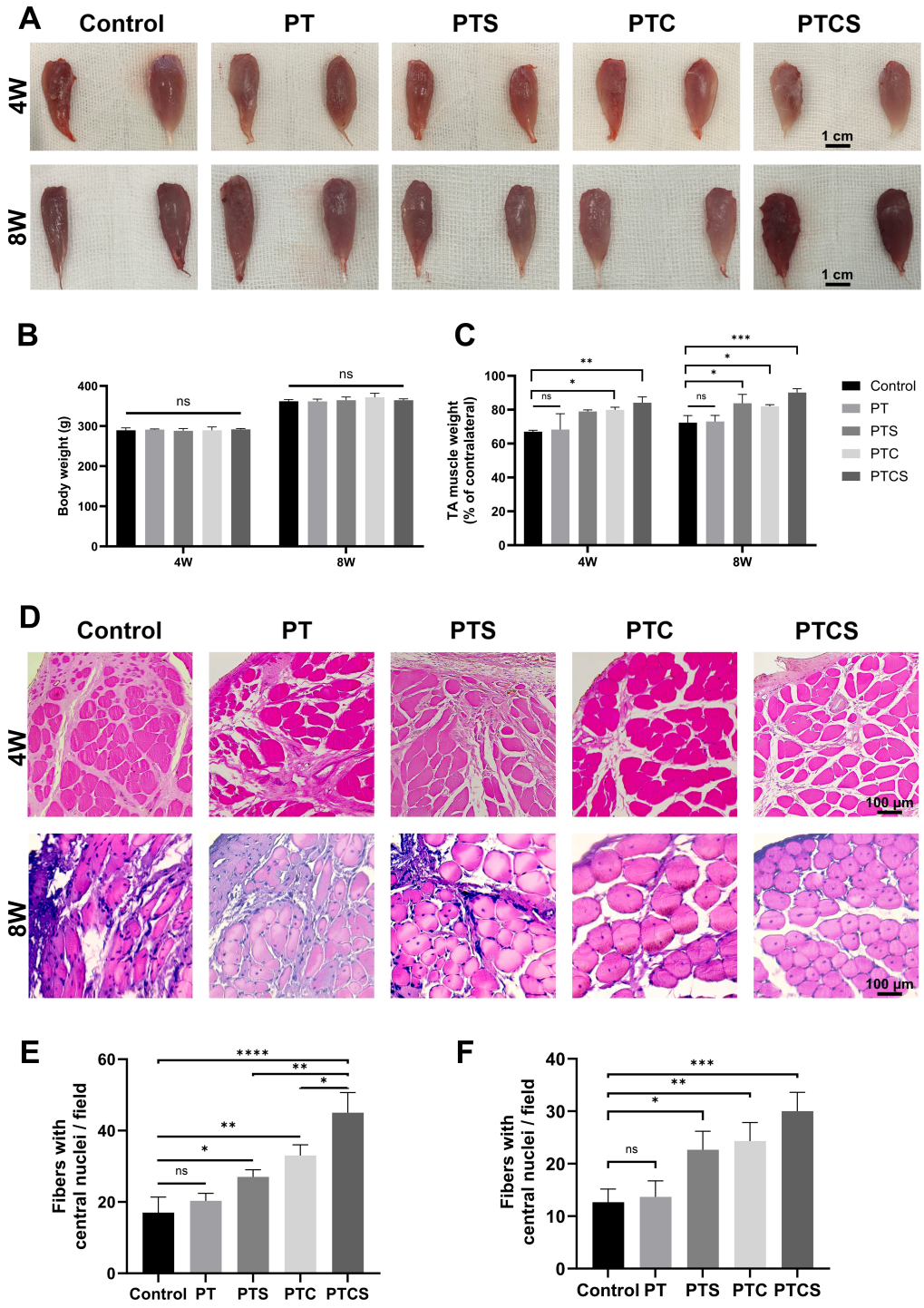

Fig. 5. PTCS improves vascularized muscle regeneration in the RTA muscle defect model. (**A**) Gross appearance of RTA muscles in different groups. Left: injured muscle. Right: contralateral muscle. Scale bars = 1 cm. (**B**) Weight of rats in different groups. (**C**) Weight of the RTA muscle in different groups. (**D**) H&E staining of the regenerated tissues of the defect sites. Scale bars = 100 μm. (**E, F**) Quantitative evaluation of regenerated myofiber density in newly-formed muscle tissue at 4- and 8-week post-implantation intervals. All data are expressed as mean ± SD (n = 3). The exact *p* value in the above multiple comparisons was calculated with one-way ANOVA Tukey's multiple comparisons test. ns: no significant difference, *$p < 0.05$, **$p < 0.01$, ***$p < 0.001$, ****$p < 0.0001$. TA, tannic acid; RTA, rat tibialis anterior; PT, PVA/TA; PTC, PVA/TA/COL I; PTS, PVA/TA/$SrCl_2$; PTCS, polyvinyl alcohol/tannic acid/COL I/Sr^{2+}; SD, standard deviation.

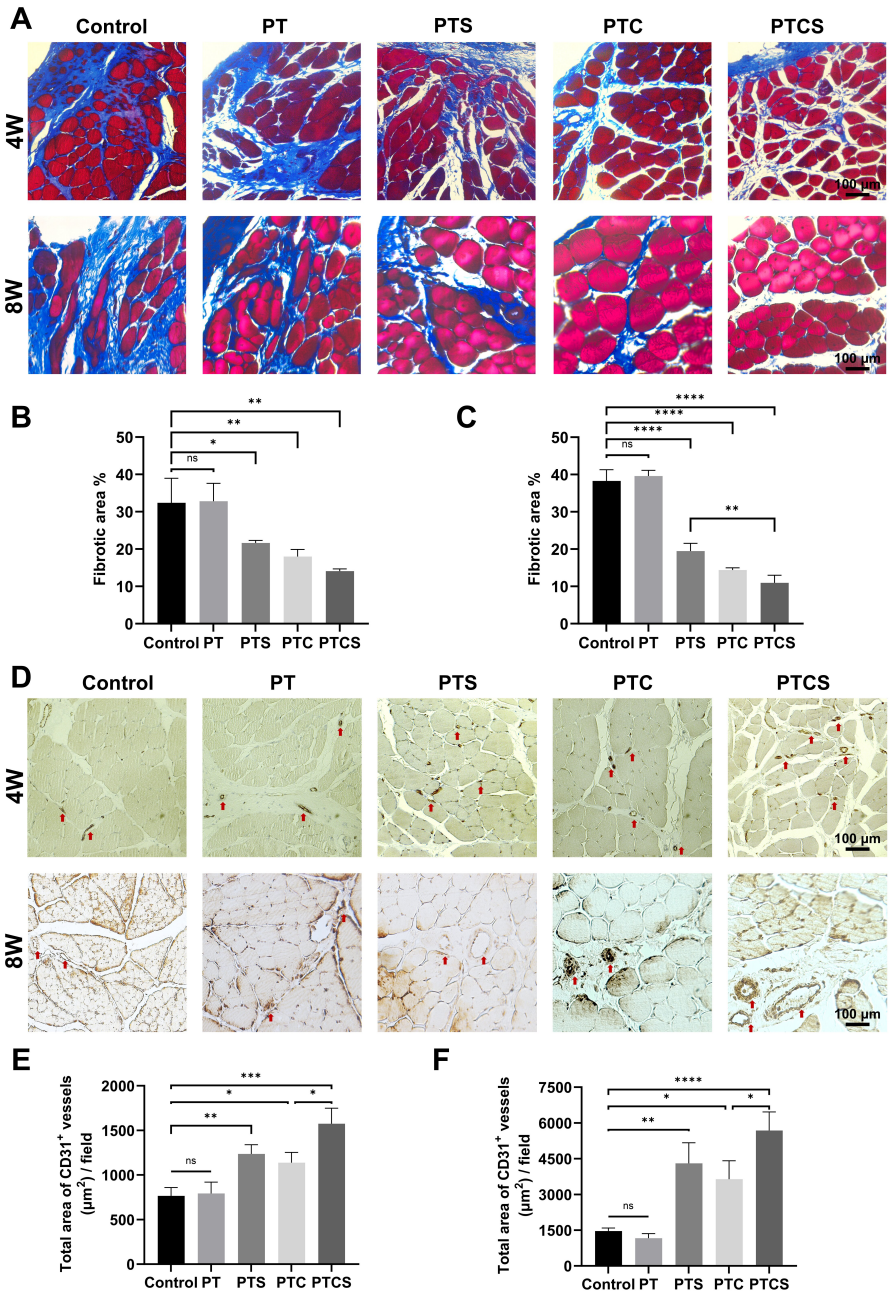

Fig. 6. PTCS improves vascularized muscle regeneration in the RTA muscle defect model. (**A**) MT staining of regenerated tissues at defect sites. Scale bars = 100 μm. (**B, C**) Quantitative analysis of the fibrotic area in the *de novo* formed tissue region at 4 and 8 weeks, respectively. (**D**) Immunohistochemical staining of CD31 expression demonstrated the vascular-specific markers (red arrow) in regenerated tissue. Scale bars = 100 μm. (**E, F**) Quantification of the total area of CD31-positive vessels per field at 4 and 8 weeks, respectively. All data are expressed as mean ± SD (n = 3). The exact *p* value in the above multiple comparisons was calculated with one-way ANOVA Tukey's multiple comparisons test. ns: no significant difference, $*p < 0.05$, $**p < 0.01$, $***p < 0.001$, $****p < 0.0001$. PT, PVA/TA; PTC, PVA/TA/COL I; PTS, PVA/TA/$SrCl_2$; PTCS, polyvinyl alcohol/tannic acid/COL I/Sr^{2+}; RTA, rat tibialis anterior; MT, Masson's trichrome; SD, standard deviation.

eration and tissue function recovery [41,42]. Mimicking the structure and function of the native ECM to provide a microenvironment similar to that *in vivo* is an effective mean for guiding and promoting tissue self-repair. Hydrogels, which are three-dimensional networks of hydrophilic polymers and more capable of simulating the ECM, have garnered considerable attention for the regeneration and repair of various tissues, including skeletal muscles [43,44]. Recently, ECM scaffolds were the most widely used natural scaffold for VML repair due to the abundance of bio-

chemical cues to enhance regeneration, and several products have already received FDA approval for soft tissue applications [45]. As a crucial component of the dECM, COL I is an ideal composition because it can support the natural microenvironment of muscle tissue [46,47]. However, its stiffness limits their effectiveness for long-term muscle culture, differentiation, and contractile force generation, which are key challenges for skeletal muscle tissue engineering applications. PVA/TA composite hydrogel is a well-proven and effective hydrogel matrix system because of its hydrogen-bonding and guaranteed strength [48].

Herein, by incorporating biofunctionalized Sr^{2+} into COL I/PVA/TA hydrogel matrix, a dual-network COL I-based hydrogel was proposed. Hydrogen bonding in hydrogels greatly improved the mechanical properties and decreased the degradation rate. The tensile stress of PTCS was significantly increased and approached the level of native murine muscle, supporting myogenic cell survival and differentiation [49,50]. The suitable stiffness allowed surgeons to cut and trim the hydrogel to match the irregular defect, which is common in current VML surgery [45]. Also, a controlled swelling can help the hydrogel to fill small gaps [51]. In muscle tissue engineering strategies, the degradation properties of bioactive materials should align with the typical regeneration duration of skeletal muscle, lasting 4-6 weeks [52]. Both PTC and PTCS exhibited degradation rates exceeding 80 % after 28 days, demonstrating suitable degradation properties for skeletal muscle repair. Considering the low dose of TA and Sr^{2+}, all components are biocompatible and commonly used in tissue engineering, and the degradation products of hydrogels are not toxic. This is supported by CCK-8 and Live/Dead staining assay results *in vitro*. Also, the *in vivo* histological results showed no sign of cytotoxicity or inflammation, confirming the biocompatibility of hydrogels. Moreover, optimal ion concentrations released from the hydrogels are beneficial to cell activity. It's been revealed that the effective concentration of Sr^{2+} is approximately 10 $\mu g \cdot mL^{-1}$ [17,53], and PTCS hydrogel containing 1 % $SrCl_2 \cdot 6H_2O$ precisely meets this requirement according to the degradation characteristics [54].

What's more, double physical crosslinking in the hydrogel avoids the toxicity associated with chemical crosslinkers while retaining the biological properties of COL I. Here, PTCS hydrogel extracts promoted the proliferation, migration, and myogenic differentiation of C2C12 myoblasts *in vitro* and increased myofibers regeneration *in vivo*. Given that the proliferation and migration levels of C2C12 myoblasts in the PTS group did not differ significantly from those in the control group, it was concluded that the promoting effect of PTCS was attributable to incorporated COL I. Previous studies have demonstrated that COL I-based bioactive ink could promote the proliferation of C2C12 myoblasts and improve the alignment of actin filaments [55]. Furthermore, COL I has also been shown to stimulate the migration and myogenic differentiation of C2C12 myoblasts through NF-κB p65-mediated upregulation of interleukin-6 secretion [8]. This study focused on the myogenic properties of the PTCS hydrogel in a mouse model of RTA muscle injury, and the RTA muscle in the PTCS group exhibited increased mass and more neoplastic myofibers with a denser arrangement and more regular morphology. These results indicated that PTCS facilitates muscle regeneration morphologically and histologically after VML injury.

The rapid recovery of blood flow, which can provide sufficient oxygen and nutrients to cells, is a key issue in repairing skeletal muscle injuries [56]. The ability of Sr^{2+} to promote angiogenesis has been demonstrated during the regeneration of different tissues, including bone [57], skin [58], and heart [59]. Many studies have reported clear positive findings that both Sr^{2+} and COL I perform well in angiogenesis tests, including *in vitro* tube formation and wound-healing assays. [60–62]. The present study demonstrated that the PTCS hydrogel significantly increased vascular density after 28 days and 56 days, indicating that Sr^{2+} and COL I both facilitated vascular regeneration after VML. Moreover, the PTCS group exhibited a markedly more efficacious therapeutic effect than the PTC and PTS groups on stimulating new blood vessel formation, indicating a synergistic effect of Sr^{2+} and COL I. Mechanistically, this synergy may reflect their partially overlapping downstream pathways. COL I has been linked to FAK/NF-κB to mediate IL-6 release and could increase VEGF expression *in vitro* [8,63]. Consistently, Sr^{2+} upregulated VEGF and activated PI3K/AKT/mTOR in HUVECs [64,65]. In addition, Sr^{2+} may promote endothelial adhesion and migration through integrin-related signaling, thereby further facilitating tube formation and vascular maturation [66]. Collagen hydrolysates could also activate this axis that was established as a central regulator of angiogenesis and muscle growth [67]. Moreover, Sr^{2+} has been reported to favor a regenerative immune microenvironment by modulating macrophage polarization toward an M2-like phenotype [68], which may enhance the secretion of pro-angiogenic and pro-myogenic factors and thereby support both angiogenesis and myogenesis [57,69]. These mechanisms provided a reasonable explanation for the superior vascularization and myogenic outcomes in PTCS. Besides, the synergistic effect of Sr^{2+} and COL I was also verified by the enhancement of the migration and invasion of HUVECs through experiments *in vitro*. Therefore, this study indicates that biomaterial systems integrated with bioactive components could play synergy effect and is a viable strategy for developing vascularization-promoting therapeutic platforms.

Collagen deposition is a contributory factor in muscle regeneration by facilitating the ECM remodeling in injured areas [70], which is essential for initiating nervous and vascular regeneration as well as satellite cells differentiation into myofibers. However, excessive or disorganized col-

lagen deposition can disrupt the migration, differentiation, and fusion of myoblast, thereby impairing proper myogenesis and normal muscle formation, eventually making it difficult to recover muscle function [71]. In this study, the control and PT groups showed a plethora of disordered collagen deposition. Relatively, the PTCS group demonstrated a notable reduction in the area of collagen deposition after VML injury, indicating that the level of fibrosis was reduced and scar formation was impeded.

In VML treatment, traditional dECM hydrogels are attractive because they retain ECM components and have been shown to support neovascularization and cell infiltration *in vivo* [72]. However, dECM hydrogels had high requirements for donor tissues and decellularization protocols, which cause variability between different batches [73]. In addition, the risk of donor morbidity and immunogenicity cannot be ignored [74]. In contrast, PTCS incorporates COL I, a fundamental ECM component, providing an ECM-mimetic interface while reducing cost and reliance on donor tissue. The PVA/TA network had muscle-like stiffness, providing consistent mechanical cues, whereas Sr^{2+} and COL I introduced biochemical cues for angiogenic and myogenic repair. Compared with ECM-mimicking hydrogels reported for muscle regeneration, such as collagen-based bioinks combined with aligned nanowires, PTCS does not rely on electrical stimulation or complex microfabrication, but instead combines simple material-level mechanical and biochemical cues in a readily deployable format [55]. Furthermore, compared with recently reported synthetic hydrogels, such as nanofiber hydrogel that enhanced mechanical strength and modulate the immune microenvironment or conductive hydrogels that introduced electroactive cues, PTCS emphasized a simple, cell- free and drug-free, safe strategy, providing mechanical and biochemical cues for muscle vascularized regeneration [75, 76].

However, some limitations should be acknowledged. First, we did not directly evaluate functional recovery after VML, such as walking track or force outputting *in vivo*, which is the most clinically meaningful measurement of treatment efficacy. Second, although our data supported a synergistic effect of COL I and Sr^{2+}, the underlying mechanism was not investigated in depth. In addition, VML repair requires effective neural regeneration and innervation because neural input supports myofiber maturation and restores motor function [77,78]. The ability of this hydrogel to facilitate nerve regeneration and restore the neuromuscular synaptic function remains to be further explored. In future work, we plan to start experiments on synergistic mechanisms and neural regeneration by assessing nerve growth and muscle force.

Conclusions

Current treatments for VML injuries have limited success and still have substantial disadvantages due to the insufficient regenerative capacity, the rapid formation of fibrosis scars, and blocked blood circulation. This study introduced a dual-network COL I-based hydrogel with sustained Sr^{2+} release to better mimic the ECM microenvironment. Specifically, this hydrogel had an appropriate stiffness (23.62 $\pm$ 0.58 kPa) and a suitable degradation rate matching the repair process of skeletal muscle. The sustained release of Sr^{2+} (11.57 $\pm$ 0.62 $\mu g \cdot mL^{-1}$), together with the presence of COL I, synergistically promoted the reconstruction of the vascular network in injured muscle *in vitro* and facilitated angiogenesis, myofiber regeneration, and reduced collagen deposition after a VML injury *in vivo*. Therefore, the composite hydrogel scaffold integrated with bioactive components mimicking ECM could be a simple treatment to facilitate muscle regeneration through synergistic effects and has great potential for converting into clinically application of vascularized muscle regeneration.

List of Abbreviations

VML, volumetric muscle loss; COL I, collagen type I; TA, tannic acid; PVA, polyvinyl alcohol; PT, PVA/TA; PTC, PVA/TA/COL I; PTS, PVA/TA/$SrCl_2$; Sr^{2+}, strontium ions; PTCS, polyvinyl alcohol/tannic acid/COL I/Sr^{2+}; ECM, extracellular matrix; dECM, decellularized extracellular matrix; DI, deionized; FBS, fetal bovine serum; FTIR, Fourier transform infrared spectroscopy; XRD, X-ray diffraction; DMEM, Dulbecco's modified Eagle's medium; HUVECs, human umbilical vein endothelial cells; SD, standard deviation; ANOVA, analysis of variance; CCK-8, Cell Counting Kit-8; RTA, rat tibialis anterior; H&E, hematoxylin and eosin; MT, Masson's trichrome; OD, optical density.

Availability of Data and Materials

The data are available from the corresponding authors on reasonable request.

Author Contributions

HCL, JT, and FCC contributed to the acquisition, analysis, and interpretation of data. FSH, HLL, and YXT contributed to the design of this work. HCL, JT, and FCC analyzed the data. HCL, JT, and FCC drafted the work. FSH, HLL, YXT, QW, KCW, and XL revised the work critically for important intellectual content. CW, ZWC, MNG, HCS, and WY collected the data and reviewed the literature. FSH, HLL, and YXT supervised the whole work and worked on funding acquisition. All authors read and approved the final manuscript. All authors agree to be accountable for all aspects of the work in ensuring that questions related to the accuracy or integrity of any part of the work are appropriately investigated and resolved.

Ethics Approval and Consent to Participate

This study has been approved by the ethics committee of Soochow University, Approval No. SUDA20241014A01. All animal procedures were performed in accordance with the Guidelines for Care and Use of Laboratory Animals of Soochow University.

Acknowledgments

Not applicable.

Funding

This work was supported by Corps science and technology program (Project No. 2022AB023), Priority Academic Program Development of Jiangsu Higher Education Institutions (PAPD), Key Laboratory of Orthopedics of Suzhou (SZS2022017), Tianshan Talent Training Project (2023TSYCJC0078), The Natural Science Foundation of Jiangsu Province (BK20240019).

Conflict of Interest

The authors declare that they have no known competing financial interests or personal relationships that could have appeared to influence the work reported in this paper.

Supplementary Material

Supplementary material associated with this article can be found, in the online version, at https://doi.org/10.22203/eCM.v058a13.

References

[1] Frontera WR, Ochala J. Skeletal muscle: a brief review of structure and function. Calcified Tissue International. 2015; 96: 183–195. https://doi.org/10.1007/s00223-014-9915-y.

[2] Gahlawat S, Oruc D, Paul N, Ragheb M, Patel S, Fasasi O, *et al*. Tissue engineered 3D constructs for volumetric muscle loss. Annals of Biomedical Engineering. 2024; 52: 2325–2347. https://doi.org/10.1007/s10439-024-03541-w.

[3] Pollot BE, Corona BT. Volumetric muscle loss. Methods in molecular biology (Clifton, N.J.). 2016; 1460: 19–31. https://doi.org/10.1007/978-1-4939-3810-0_2.

[4] Novakova SS, Rodriguez BL, Vega-Soto EE, Nutter GP, Armstrong RE, Macpherson PCD, *et al*. Repairing Volumetric Muscle Loss in the Ovine Peroneus Tertius Following a 3-Month Recovery. Tissue engineering. Part A. 2020; 26: 837–851. https://doi.org/10.1089/ten.TEA.2019.0288.

[5] Collins J, Ayeni O, Thoma A. A systematic review of anterolateral thigh flap donor site morbidity. The Canadian journal of plastic surgery. 2012; 20: 17–23. https://doi.org/10.1177/229255031202000103.

[6] Wang Q, Ji J, Huang D, Gao C. Biomaterials for Modulating the Immune Microenvironment in Rheumatoid Arthritis. BME Frontiers. 2025; 6: 0102. https://doi.org/10.34133/bmef.0102.

[7] Chen CL, Wei SY, Chen WL, Hsu TL, Chen YC. Reconstructing vascular networks promotes the repair of skeletal muscle following volumetric muscle loss by pre-vascularized tissue constructs. Journal of Tissue Engineering. 2023; 14: 20417314231201231. https://doi.org/10.1177/20417314231201231.

[8] Liu X, Gao Y, Long X, Hayashi T, Mizuno K, Hattori S, *et al*. Type I collagen promotes the migration and myogenic differentiation of C2C12 myoblasts via the release of interleukin-6 mediated by FAK/NF-κB p65 activation. Food & Function. 2020; 11: 328–338. https://doi.org/10.1039/c9fo01346f.

[9] Carleton MM, Locke M, Sefton MV. Methacrylic acid-based hydrogels enhance skeletal muscle regeneration after volumetric muscle loss in mice. Biomaterials. 2021; 275: 120909. https://doi.org/10.1016/j.biomaterials.2021.120909.

[10] Li H, Li JM, Li T, Wu CW, Zhang W. Macroporous polyvinyl alcohol-tannic acid hydrogel with high strength and toughness for cartilage replacement. Journal of Materials Science. 2022; 57: 8262–8275. https://doi.org/10.1007/s10853-022-07209-5.

[11] Zhuo H, Dong X, Liu Q, Hong L, Zhang Z, Long S, *et al*. Bamboo-inspired ultra-strong nanofiber-reinforced composite hydrogels. Nature Communications. 2025; 16: 980. https://doi.org/10.1038/s41467-025-56340-9.

[12] Latroche C, Gitiaux C, Chrétien F, Desguerre I, Mounier R, Chazaud B. Skeletal muscle microvasculature: a highly dynamic lifeline. Physiology (Bethesda, Md.). 2015; 30: 417–427. https://doi.org/10.1152/physiol.00026.2015.

[13] Jacobsen NL, Morton AB, Segal SS. Angiogenesis precedes myogenesis during regeneration following biopsy injury of skeletal muscle. Skeletal Muscle. 2023; 13: 3. https://doi.org/10.1186/s13395-023-00313-3.

[14] Namjoo AR, Abrbekoh FN, Saghati S, Amini H, Saadatlou MAE, Rahbarghazi R. Tissue engineering modalities in skeletal muscles: focus on angiogenesis and immunomodulation properties. Stem Cell Research & Therapy. 2023; 14: 90. https://doi.org/10.1186/s13287-023-03310-x.

[15] Mao L, Xia L, Chang J, Liu J, Jiang L, Wu C, *et al*. The synergistic effects of Sr and Si bioactive ions on osteogenesis, osteoclastogenesis and angiogenesis for osteoporotic bone regeneration. Acta Biomaterialia. 2017; 61: 217–232. https://doi.org/10.1016/j.actbio.2017.08.015.

[16] Jebahi S, Oudadesse H, Jardak N, Khayat I, Keskes H, Khabir A, *et al*. Biological therapy of strontium-substituted bioglass for soft tissue wound-healing: responses to oxidative stress in ovariectomised rats. Annales Pharmaceutiques Françaises. 2013; 71: 234–242. https://doi.org/10.1016/j.pharma.2013.05.003.

[17] Yuan Y, Zhang Z, Mo F, Yang C, Jiao Y, Wang E, *et al*. A biomaterial-based therapy for lower limb ischemia using Sr/Si bioactive hydrogel that inhibits skeletal muscle necrosis and enhances angiogenesis. Bioactive Materials. 2023; 26: 264–278. https://doi.org/10.1016/j.bioactmat.2023.02.027.

[18] Grasman JM, Zayas MJ, Page RL, Pins GD. Biomimetic scaffolds for regeneration of volumetric muscle loss in skeletal muscle injuries. Acta biomaterialia. 2015; 25: 2–15. https://doi.org/10.1016/j.actbio.2015.07.038.

[19] Wu X, Corona BT, Chen X, Walters TJ. A standardized rat model of volumetric muscle loss injury for the development of tissue engineering therapies. BioResearch open access. 2012; 1: 280–290. https://doi.org/10.1089/biores.2012.0271.

[20] Daskalakis E, Hassan MH, Omar AM, Acar AA, Fallah A, Cooper G, *et al*. Accelerated Degradation of Poly-ϵ-caprolactone Composite Scaffolds for Large Bone Defects. Polymers. 2023; 15: 670. https://doi.org/10.3390/polym15030670.

[21] Li J, Mooney DJ. Designing hydrogels for controlled drug delivery. Nature reviews. Materials. 2016; 1: 16071. https://doi.org/10.1038/natrevmats.2016.71.

[22] Cheng M, Hu L, Xu G, Pan P, Liu Q, Zhang Z, *et al*. Tannic acid-based dual-network homogeneous hydrogel with antimicrobial and pro-healing properties for infected wound healing. Colloids and surfaces. B, Biointerfaces. 2023; 227: 113354. https://doi.org/10.1016/j.colsurfb.2023.113354.

[23] Liang X, Zhong HJ, Ding H, Yu B, Ma X, Liu X, *et al*. Polyvinyl Alcohol (PVA)-Based Hydrogels: Recent Progress in Fabrication,

Properties, and Multifunctional Applications. Polymers. 2024; 16: 2755. https://doi.org/10.3390/polym16192755.

[24] Ozmen MM, Okay O. Superfast responsive ionic hydrogels with controllable pore size. Polymer. 2005; 46: 8119–8127. https://doi.org/10.1016/j.polymer.2005.06.102.

[25] Song X, Philpott MA, Best SM, Cameron RE. Controlling the Architecture of Freeze-Dried Collagen Scaffolds with Ultrasound-Induced Nucleation. Polymers. 2024; 16: 213. https://doi.org/10.3390/polym16020213.

[26] Pawelec KM, Husmann A, Wardale RJ, Best SM, Cameron RE. Ionic solutes impact collagen scaffold bioactivity. Journal of materials science. Materials in medicine. 2015; 26: 91. https://doi.org/10.1007/s10856-015-5457-8.

[27] Xia P, Luo Y. Vascularization in tissue engineering: the architecture cues of pores in scaffolds. Journal of biomedical materials research. Part B, Applied biomaterials. 2022; 110: 1206–1214. https://doi.org/10.1002/jbm.b.34979.

[28] Boonen KJ, Rosaria-Chak KY, Baaijens FP, van der Schaft DW, Post MJ. Essential environmental cues from the satellite cell niche: optimizing proliferation and differentiation. American Journal of Physiology – Cell Physiology. 2009; 296: C1338–C1345. https://doi.org/10.1152/ajpcell.00015.2009.

[29] Xie W, Guo Z, Zhao L, Wei Y. Metal-phenolic networks: facile assembled complexes for cancer theranostics. Theranostics. 2021; 11: 6407–6426. https://doi.org/10.7150/thno.58711.

[30] Jana S, Levengood SK, Zhang M. Anisotropic Materials for Skeletal-Muscle-Tissue Engineering. Advanced materials (Deerfield Beach, Fla.). 2016; 28: 10588–10612. https://doi.org/10.1002/adma.201600240.

[31] Mathur AB, Collinsworth AM, Reichert WM, Kraus WE, Truskey GA. Endothelial, cardiac muscle and skeletal muscle exhibit different viscous and elastic properties as determined by atomic force microscopy. Journal of biomechanics. 2001; 34: 1545–1553. https://doi.org/10.1016/s0021-9290(01)00149-x.

[32] Tan YH, Habing KM, Riesterer JL, Stempinski ES, Lewis SH, Pfeifer CS, *et al*. Engineered nanofibrillar collagen with tunable biophysical properties for myogenic, endothelial, and osteogenic cell guidance. Acta Biomaterialia. 2024; 186: 95–107. https://doi.org/10.1016/j.actbio.2024.08.002.

[33] Herbanu A, Ana ID, Ardhani R, Siswomihardjo W. Fibrous PVA Matrix Containing Strontium-Substituted Hydroxyapatite Nanoparticles from Golden Apple Snail (Pomacea canaliculata L.) Shells for Bone Tissue Engineering. Bioengineering (Basel, Switzerland). 2023; 10: 844. https://doi.org/10.3390/bioengineering10070844.

[34] Zhang F, Wu J, Kang D, Zhang H. Development of a complex hydrogel of hyaluronan and PVA embedded with silver nanoparticles and its facile studies on Escherichia coli. Journal of biomaterials science. Polymer edition. 2013; 24: 1410–1425. https://doi.org/10.1080/09205063.2012.763109.

[35] Jensen BE, Dávila I, Zelikin AN. Poly (vinyl alcohol) Physical Hydrogels: Matrix-Mediated Drug Delivery Using Spontaneously Eroding Substrate. The journal of physical chemistry. B. 2016; 120: 5916–5926. https://doi.org/10.1021/acs.jpcb.6b01381.

[36] Ng HW, Zhang Y, Naffa R, Prabakar S. Monitoring the Degradation of Collagen Hydrogels by Collagenase Clostridium histolyticum. Gels (Basel, Switzerland). 2020; 6: 46. https://doi.org/10.3390/gels6040046.

[37] Velmurugan P, Singam ER, Jonnalagadda RR, Subramanian V. Investigation on interaction of tannic acid with type I collagen and its effect on thermal, enzymatic, and conformational stability for tissue engineering applications. Biopolymers. 2014; 101: 471–483. https://doi.org/10.1002/bip.22405.

[38] Dey K, Agnelli S, Borsani E, Sartore L. Degradation-Dependent Stress Relaxing Semi-Interpenetrating Networks of Hydroxyethyl Cellulose in Gelatin-PEG Hydrogel with Good Mechanical Stability and Reversibility. Gels (Basel, Switzerland). 2021; 7: 277. https://doi.org/10.3390/gels7040277.

[39] Asakura A, Kikyo N. Immunofluorescence analysis of myogenic differentiation. Methods in Cell Biology. 2022; 170: 117–125. https://doi.org/10.1016/bs.mcb.2022.02.010.

[40] Järvinen TA, Järvinen TL, Kääriäinen M, Kalimo H, Järvinen M. Muscle injuries: biology and treatment. The American journal of sports medicine. 2005; 33: 745–764. https://doi.org/10.1177/0363546505274714.

[41] Alheib O, da Silva LP, Caballero D, Pires RA, Kundu SC, Correlo VM, *et al*. Micropatterned gellan gum-based hydrogels tailored with laminin-derived peptides for skeletal muscle tissue engineering. Biomaterials. 2021; 279: 121217. https://doi.org/10.1016/j.biomaterials.2021.121217.

[42] Eugenis I, Wu D, Rando TA. Cells, scaffolds, and bioactive factors: engineering strategies for improving regeneration following volumetric muscle loss. Biomaterials. 2021; 278: 121173. https://doi.org/10.1016/j.biomaterials.2021.121173.

[43] Chen Z, Huang Y, Xing H, Tseng T, Edelman H, Perry R, *et al*. Novel muscle-derived extracellular matrix hydrogel promotes angiogenesis and neurogenesis in volumetric muscle loss. Matrix Biology. 2024; 127: 38–47. https://doi.org/10.1016/j.matbio.2024.02.001.

[44] Pantelic MN, Larkin LM. Stem cells for skeletal muscle tissue engineering. Tissue engineering. Part B, Reviews. 2018; 24: 373–391. https://doi.org/10.1089/ten.TEB.2017.0451.

[45] Dziki J, Badylak S, Yabroudi M, Sicari B, Ambrosio F, Stearns K, *et al*. An acellular biologic scaffold treatment for volumetric muscle loss: results of a 13-patient cohort study. NPJ Regenerative Medicine. 2016; 1: 16008. https://doi.org/10.1038/npjregenmed.2016.8.

[46] Kessler JL, Kang G, Qin Z, Kang H, Whitby FG, Cheatham TE 3rd, *et al*. Peptoid residues make diverse, hyperstable collagen triple-helices. Journal of the American Chemical Society. 2021; 143: 10910–10919. https://doi.org/10.1021/jacs.1c00708.

[47] Shin DS, Schroeder ME, Anseth KS. Impact of collagen triple helix structure on melanoma cell invadopodia formation and matrix degradation upon BRAF inhibitor treatment. Advanced Healthcare Materials. 2022; 11: e2101592. https://doi.org/10.1002/adhm.202101592.

[48] Chen YN, Peng L, Liu T, Wang Y, Shi S, Wang H. Poly (vinyl alcohol)-Tannic Acid Hydrogels with Excellent Mechanical Properties and Shape Memory Behaviors. ACS applied materials & interfaces. 2016; 8: 27199–27206. https://doi.org/10.1021/acsami.6b08374.

[49] Engler AJ, Sen S, Sweeney HL, Discher DE. Matrix elasticity directs stem cell lineage specification. Cell. 2006; 126: 677–689. https://doi.org/10.1016/j.cell.2006.06.044.

[50] Sleep E, Cosgrove BD, McClendon MT, Preslar AT, Chen CH, Sangji MH, *et al*. Injectable biomimetic liquid crystalline scaffolds enhance muscle stem cell transplantation. Proceedings of the National Academy of Sciences of the United States of America. 2017; 114: E7919–E7928. https://doi.org/10.1073/pnas.1708142114.

[51] Alcazar CA, Hu C, Rando TA, Huang NF, Nakayama KH. Transplantation of insulin-like growth factor-1 laden scaffolds combined with exercise promotes neuroregeneration and angiogenesis in a preclinical muscle injury model. Biomaterials Science. 2020; 8: 5376–5389. https://doi.org/10.1039/d0bm00990c.

[52] Truskey GA. Development and application of human skeletal muscle microphysiological systems. Lab on a Chip. 2018; 18: 3061–3073. https://doi.org/10.1039/c8lc00553b.

[53] Fernandes G, Vanyo ST, Alsharif SBA, Andreana S, Visser MB, Dziak R. Strontium effects on human gingival fibroblasts. The Journal of oral implantology. 2019; 45: 274–280. https://doi.org/10.1563/aaid-joi-D-18-00253.

[54] Pontremoli C, Boffito M, Laurano R, Iviglia G, Torre E, Cassinelli C, *et al*. Mesoporous bioactive glasses incorporated into an injectable thermosensitive hydrogel for sustained co-release of Sr^{2+} ions and

N-acetylcysteine. Pharmaceutics. 2022; 14: 1890. https://doi.org/10.3390/pharmaceutics14091890.

[55] Kim W, Jang CH, Kim GH. A myoblast-laden collagen bioink with fully aligned Au nanowires for muscle-tissue regeneration. Nano Letters. 2019; 19: 8612–8620. https://doi.org/10.1021/acs.nanolett.9b03182.

[56] Forster R, Liew A, Bhattacharya V, Shaw J, Stansby G. Gene therapy for peripheral arterial disease. The Cochrane database of systematic reviews. 2018; 10: CD012058. https://doi.org/10.1002/14651858.CD012058.pub2.

[57] Chen T, Wu X, Zhang P, Wu W, Dai H, Chen S. Strontium-doped hydroxyapatite coating improves osteo/angiogenesis for ameliorative graft-bone integration via the macrophage-derived cytokines-mediated integrin signal pathway. ACS Applied Materials & Interfaces. 2024; 16: 15687–15700. https://doi.org/10.1021/acsami.3c14904.

[58] Chen Y, Ye M, Wang X, Li W, Chen W. Corrigendum to 'Functionalized gelatin/strontium hydrogel bearing endothelial progenitor cells for accelerating angiogenesis in wound tissue regeneration' [Biomater. Adv. 136 (2022) 212803]. Biomaterials Advances. 2025; 174: 214318. https://doi.org/10.1016/j.bioadv.2025.214318.

[59] Xing M, Jiang Y, Bi W, Gao L, Zhou YL, Rao SL, *et al*. Strontium ions protect hearts against myocardial ischemia/reperfusion injury. Science Advances. 2021; 7: eabe0726. https://doi.org/10.1126/sciadv.abe0726.

[60] Fu YJ, Shi YF, Wang LY, Zhao YF, Wang RK, Li K, *et al*. All-natural immunomodulatory bio-adhesive hydrogel promotes angiogenesis and diabetic wound healing by regulating macrophage heterogeneity. Advanced science (Weinheim, Baden-Württemberg, Germany). 2023; 10: e2206771. https://doi.org/10.1002/advs.202206771.

[61] Shan Y, Bai Y, Zhao L, Zhou Q, Yang S, Wang G, *et al*. Three-dimensional-printed strontium-incorporated β-TCP bioceramic triply periodic minimal surface scaffolds with enhanced angiogenic and osteogenic properties. Regenerative biomaterials. 2025; 12: rbaf080. https://doi.org/10.1093/rb/rbaf080.

[62] Nakamura J, Shigematsu S, Yamauchi K, Takeda T, Yamazaki M, Kakizawa T, *et al*. Biphasic function of focal adhesion kinase in endothelial tube formation induced by fibril-forming collagens. Biochemical and biophysical research communications. 2008; 374: 699–703. https://doi.org/10.1016/j.bbrc.2008.07.123.

[63] Imai H, Honda S, Kondo N, Ishibashi K, Tsukahara Y, Negi A. The upregulation of angiogenic gene expression in cultured retinal pigment epithelial cells grown on type I collagen. Current eye research. 2007; 32: 903–910. https://doi.org/10.1080/02713680701604749.

[64] Guo X, Wei S, Lu M, Shao Z, Lu J, Xia L, *et al*. Dose-dependent Effects of Strontium Ranelate on Ovariectomy Rat Bone Marrow Mesenchymal Stem Cells and Human Umbilical Vein Endothelial Cells. International journal of biological sciences. 2016; 12: 1511–1522. https://doi.org/10.7150/ijbs.16499.

[65] Miao Q, Yang X, Diao J, Ding H, Wu Y, Ren X, *et al*. 3D printed strontium-doped calcium phosphate ceramic scaffold enhances early angiogenesis and promotes bone repair through the regulation of macrophage polarization. Materials today. Bio. 2023; 23: 100871. https://doi.org/10.1016/j.mtbio.2023.100871.

[66] Lu W, Zhou C, Ma Y, Li J, Jiang J, Chen Y, *et al*. Improved osseointegration of strontium-modified titanium implants by regulating angiogenesis and macrophage polarization. Biomaterials Science. 2022; 10: 2198–2214. https://doi.org/10.1039/d1bm01488a.

[67] Kitakaze T, Sakamoto T, Kitano T, Inoue N, Sugihara F, Harada N, *et al*. The collagen derived dipeptide hydroxyprolyl-glycine promotes C2C12 myoblast differentiation and myotube hypertrophy. Biochemical and biophysical research communications. 2016; 478: 1292–1297. https://doi.org/10.1016/j.bbrc.2016.08.114.

[68] Zhou J, Jiang S, Wang L, Lin K, Wu J, Gui H, *et al*. Decellularized Adipose Matrix Rejuvenates Photoaged Skin through Immune Microenvironment Modulation. BME Frontiers. 2025; 6: 0166. https://doi.org/10.34133/bmef.0166.

[69] Liu X, Huang H, Zhang J, Sun T, Zhang W, Li Z. Recent Advance of Strontium Functionalized in Biomaterials for Bone Regeneration. Bioengineering (Basel, Switzerland). 2023; 10: 414. https://doi.org/10.3390/bioengineering10040414.

[70] Chen WJ, Lin IH, Lee CW, Chen YF. Aged skeletal muscle retains the ability to remodel extracellular matrix for degradation of collagen deposition after muscle injury. International Journal of Molecular Sciences. 2021; 22: 2123. https://doi.org/10.3390/ijms22042123.

[71] Brack AS, Conboy MJ, Roy S, Lee M, Kuo CJ, Keller C, *et al*. Increased Wnt signaling during aging alters muscle stem cell fate and increases fibrosis. Science (New York, N.Y.). 2007; 317: 807–810. https://doi.org/10.1126/science.1144090.

[72] Shuai QZ, Cheng JW, Wang XW, Li XL, Xu K, Ge M, *et al*. Adipose-derived EVs loaded resolvins biopotentiated decellularized extracellular matrix hydrogels accelerate muscle regeneration. Chemical Engineering Journal. 2025; 514: 163325. https://doi.org/10.1016/j.cej.2025.163325.

[73] DeQuach JA, Lin JE, Cam C, Hu D, Salvatore MA, Sheikh F, *et al*. Injectable skeletal muscle matrix hydrogel promotes neovascularization and muscle cell infiltration in a hindlimb ischemia model. European cells & materials. 2012; 23: 400–412. https://doi.org/10.22203/ecm.v023a31.

[74] Langridge B, Griffin M, Butler PE. Regenerative medicine for skeletal muscle loss: a review of current tissue engineering approaches. Journal of materials science. Materials in medicine. 2021; 32: 15. https://doi.org/10.1007/s10856-020-06476-5.

[75] Yu W, Zhang X, Gu M, Wang J, Zhang Y, Zhang W, *et al*. Bioactive Nanofiber-Hydrogel Composite Regulates Regenerative Microenvironment for Skeletal Muscle Regeneration after Volumetric Muscle Loss. Advanced healthcare materials. 2024; 13: e2304087. https://doi.org/10.1002/adhm.202304087.

[76] Shi MT, Dong RA, Hu J, Guo BL. Conductive self-healing biodegradable hydrogel based on hyaluronic acid-grafted-polyaniline as cell recruitment niches and cell delivery carrier for myogenic differentiation and skeletal muscle regeneration. Chemical Engineering Journal. 2023; 457: 141110. https://doi.org/10.1016/j.cej.2022.141110.

[77] Joshi A, Choudhury S, Baghel VS, Ghosh S, Gupta S, Lahiri D, *et al*. 4D Printed Programmable Shape-Morphing Hydrogels as Intraoperative Self-Folding Nerve Conduits for Sutureless Neurorrhaphy. Advanced healthcare materials. 2023; 12: e2300701. https://doi.org/10.1002/adhm.202300701.

[78] Gilbert-Honick J, Iyer SR, Somers SM, Takasuka H, Lovering RM, Wagner KR, *et al*. Engineering 3D skeletal muscle primed for neuromuscular regeneration following volumetric muscle loss. Biomaterials. 2020; 255: 120154. https://doi.org/10.1016/j.biomaterials.2020.120154.

Editor's note: The Scientific Editors responsible for this paper were Pengyuan Wang and Kelong Fan.

Received: 26th August 2025; **Accepted**: 27th May 2026; **Published**: 31st August 2026